CrossMark

The Orbit of Warm Jupiter WASP-106 b is Aligned with its Star

Jan-Vincent Harre[1] , Alexis M. S. Smith[1] , Teruyuki Hirano[2,3,4] , Szilárd Csizmadia[1] , Amaury H. M. J. Triaud[5] , and
David R. Anderson[6,7]

[1] Institute of Planetary Research, German Aerospace Center (DLR), Rutherfordstraße 2, D-12489 Berlin, Germany
[2] Astrobiology Center, 2-21-1 Osawa, Mitaka, Tokyo 181-8588, Japan
[3] National Astronomical Observatory of Japan, 2-21-1 Osawa, Mitaka, Tokyo 181-8588, Japan
[4] Department of Astronomical Science, School of Physical Sciences, The Graduate University for Advanced Studies (SOKENDAI), 2-21-1, Osawa, Mitaka, Tokyo, 181-8588, Japan
[5] School of Physics & Astronomy, University of Birmingham, Edgbaston, Birmingham B15 2TT, UK
[6] Centre for Exoplanets and Habitability, University of Warwick, Coventry CV4 7AL, UK
[7] Department of Physics, University of Warwick, Coventry CV4 7AL, UK

Abstract

Understanding orbital obliquities, or the misalignment angles between a star's rotation axis and the orbital axis of its planets, is crucial for unraveling the mechanisms of planetary formation and migration. In this study, we present an analysis of Rossiter–McLaughlin (RM) observations of the warm Jupiter exoplanet WASP-106 b. The high-precision radial velocity measurements were made with HARPS and HARPS-N during the transit of this planet. We aim to constrain the orientation of the planet's orbit relative to its host star's rotation axis. The RM observations are analyzed using a code which models the RM anomaly together with the Keplerian orbit given several parameters in combination with a Markov chain Monte Carlo implementation. We measure the projected stellar obliquity in the WASP-106 system for the first time and find $\lambda = (-1 \pm 11)°$, supporting the theory of quiescent migration through the disk.

Unified Astronomy Thesaurus concepts: Exoplanet evolution (491); Exoplanet migration (2205); Radial velocity (1332); Photometry (1234); Transits (1711)

1. Introduction

The diversity of exoplanetary systems has unveiled a wealth of information about the complex interplay between planets and their host stars. One key aspect that has captured considerable attention in recent years is the obliquity of planetary orbits, which plays a major role in understanding the mechanisms governing planetary formation, migration, and long-term stability. The projected obliquity, defined as the misalignment angle between the stellar rotation axis and the planetary orbital axis, offers valuable insights into the dynamical history of these systems.

In recent years, studies focusing on hot and warm Jupiter systems have revealed a wide range of obliquity measurements, with some planets exhibiting near perfect alignment with their host star's equator (e.g., Fulton et al. 2013; Anderson et al. 2015; Esposito et al. 2017; Lund et al. 2017; Wong et al. 2021), while others display significant misalignments, including polar or even retrograde orbits (e.g., Bayliss et al. 2010; Hébrard et al. 2011; Albrecht et al. 2012; Esposito 2014; Crouzet et al. 2017; Ahlers et al. 2020). These observations have led to various theories regarding the formation and subsequent migration processes of these gas giants. However, hot Jupiters are seemingly misplaced by high-eccentricity migration, with spin–orbit misalignments being able to be reverted by tidal damping (Rice et al. 2022a) if they are orbiting cool stars. For hot hosts ($T_{eff} > 6250$ K) of hot Jupiters it is suggested that due to their thinner convective zones they are not able to realign misaligned orbits efficiently (Winn et al. 2010).

Warm Jupiters, especially those in single star systems, orbit preferentially in alignment with their host star's rotation (Rice et al. 2022b), even though there has recently been a discovery of a warm Jupiter with a significant misalignment of $\lambda = 38.9^{+2.8}_{-2.7}°$ and eccentricity ($e = 0.57^{+0.12}_{-0.16}$) (Dong et al. 2023). Understanding the origins of such diverse obliquity distributions and their implications for planetary migration mechanisms remain active areas of research. For a recent review on stellar obliquities see, e.g., Albrecht et al. (2022).

Lately, there have been numerous measurements of the true 3D obliquities that require the stellar inclination to be measured in addition to the projected obliquity; see, e.g., Cegla et al. (2016), Bourrier et al. (2023), and Doyle et al. (2023). Depending on the orientation of the stellar spin axis with regard to our line of sight to the observed system, the projected and 3D obliquity can be quite different from one another (see e.g., Hixenbaugh et al. 2023).

In this paper, we present an investigation into the projected obliquity of one warm Jupiter, namely WASP-106 b, utilizing a combination of high-precision radial velocity (RV) measurements and the Rossiter–McLaughlin (RM) effect (McLaughlin 1924; Rossiter 1924). By analyzing the stellar radial velocity variations during planetary transit, we aim to derive a precise measurement of the projected obliquity for this system. This is particularly interesting for the examined system, since the host star's effective temperature is just at the Kraft break (Kraft 1967), which separates stars with deep and shallow convective zones. These measurements offer valuable constraints on the orientations of the planetary orbits and provide insights into their formation histories, migration pathways, and subsequent dynamical evolution.

Our study contributes to the growing body of knowledge surrounding obliquity measurements and their significance in

Table 1
Summary of Stellar Properties of WASP-106

Parameter	Value	Source
R.A. (J2000)	11:05:43.14	Simbad
Decl. (J2000)	-05:04:45.94	Simbad
$\mu_{\text{R.A.}}$ (mas yr^{-1})	-24.73	Gaia DR3
$\mu_{\text{decl.}}$ (mas yr^{-1})	-13.13	Gaia DR3
Age (Gyr)	7 ± 2	Borsato et al. (2021)
Parallax (mas)	2.783 ± 0.018	Gaia DR3
Distance (pc)	$351.8^{+2.0}_{-2.2}$	Gaia DR3
V (mag)	11.21	Simbad
G (mag)	11.36	Gaia DR3
Spectral type	F9 D	Simbad
T_{eff} (K)	6265 ± 36	Borsato et al. (2021)
$v \sin i$ (km s^{-1})	6.3 ± 0.7	Smith et al. (2014)
$\log g$	$4.38^{+0.04}_{-0.04}$	Borsato et al. (2021)
$\rho_\star$ ($\rho_\odot$)	0.81 ± 0.15	Borsato et al. (2021)
[Fe/H] (dex)	0.15 ± 0.03	Borsato et al. (2021)
$R_\star$ ($R_\odot$)	1.42 ± 0.02	Borsato et al. (2021)
$M_\star$ ($M_\odot$)	1.26 ± 0.05	Borsato et al. (2021)

Table 2
Observation Log for Rossiter–McLaughlin Observations for our Target
WASP-106 b

Instrument	Night	Exposures	Program ID
HARPS	2014-04-03	21	093.C-0474(A)
HARPS	2015-01-16	33	094.C-0090(A)
HARPS-N	2015-02-13	48	OPT14B_66

Note. These data are freely available at the TNG archive (http://archives.ia2.inaf.it/tng/) in the case of HARPS-N and at the ESO archive (http://archive.eso.org/eso/eso_archive_main.html) for HARPS observations.

the context of planetary systems. By focusing on warm Jupiter exoplanets, we aim to deepen our understanding of the mechanisms that govern the formation and migration of these gas giants in close proximity to their host stars. Through this research, we want to find out how these systems acquired their observed obliquities and the role played by various dynamical processes in shaping their architectures.

Overall, this work represents a step forward in characterizing the obliquity distributions of warm Jupiter systems—by expanding the limited sample of about 16 measured obliquities of warm Jupiters (see e.g., Mancini et al. 2022; Rice et al. 2022b; Dong et al. 2023; Sedaghati et al. 2023)—and provides valuable insights into the complex interplay between planetary migration, dynamical interactions, and the properties of host stars.

In Section 2 we describe the set of observations that are used in our analysis. Section 3 gives information about our RM modeling code, with the results presented in Section 4 and discussed in Section 5. The conclusions are given in Section 6.

2. Observations

2.1. System Parameters

The stellar host of WASP-106 b is an F9-type star. The warm Jupiter in this system is on a 9.29 days orbit, has a mass of two times that of Jupiter, and was discovered by Smith et al. (2014). A summary of the stellar parameters can be found in Table 1.

2.2. Radial Velocity Data

We obtained archival HARPS[8] (Mayor et al. 2003) and HARPS-N[9] (Cosentino et al. 2012) RM observations, which are described in Table 2, for our target, as well as further publicly available out-of-transit data from the literature. In addition to the RM observations, for WASP-106 b, there are 29 RVs available in Smith et al. (2014). Of these, 20 observations were obtained using the CORALIE spectrograph (Queloz et al. 2000) and nine using the SOPHIE spectrograph

(Perruchot et al. 2008), all of which were taken between 2013 January and 2014 February. The radial velocity data can be found in Table 4.

2.3. Photometric Data

In addition, the investigated system has been observed by Transiting Exoplanet Survey Satellite (TESS).[10] WASP-106 was observed in Sectors 9, 36, 45, and 46. The cadences are 120 s each, except for the Sector 36 observations, where data with a cadence of 20 s are also available.

3. Modeling

3.1. Radial Velocities

To fit the observed RVs during and out of transit, we used a C++ script, which implements the analytic calculation for the RM effect by Hirano et al. (2011) in addition to the standard RV curve from the Keplerian orbit of the planet. Based on the assumption that the RVs are derived by the template-matching technique as for, e.g., the HARPS Data Reduction Software (DRS) or SERVAL (Zechmeister et al. 2018), the script returns the velocity anomaly due to the RM effect and the Keplerian orbit for a set of times sampled. The input parameters to the script are all RV, RM and transit parameters, namely the RV amplitude K, the eccentricity e and argument of periastron ω as $\sqrt{e} \sin(\omega)$ and $\sqrt{e} \cos(\omega)$, the stellar rotational velocity $v \sin i$, the projected stellar obliquity angle λ, the quadratic limb-darkening parameters u_1 and u_2, the RV offset γ, the transit center time T_c, the scaled semimajor axis $a\,R_\star^{-1}$, impact parameter b, planet-to-star radius ratio $R_p\,R_\star^{-1}$, planetary orbital period P, the number of discrete times at which to compute the model, and, lastly, the discrete times at which to evaluate the model. The macroturbulent velocity ζ needed to compute the analytic RM model is set to 3.8 km s^{-1} (Gray 1977, 2018) as WASP-106 is a solar-type star. The RM model from the modeling code is then optimized to fit to our data using an Markov chain Monte Carlo (MCMC) algorithm, implemented using the *emcee Python* package (Foreman-Mackey et al. 2013). We use 100 walkers with 25.000 steps and a burn-in period of 5000 steps. To ensure convergence, we compute the autocorrelation time and compare it to the number of steps divided by 50. In our MCMC optimization, we used Gaussian priors from the discovery and follow-up paper, except for the midtransit time T_c and orbital period P, which we infer from the TESS photometry, and the projected stellar obliquity λ and the specific RV offsets γ_i where we apply uniform priors,

---

[8] Freely available at the ESO archive http://archive.eso.org/.
[9] Freely available at the TNG archive http://archives.ia2.inaf.it/.

[10] These data are publicly available at the MAST Portal under 10.17909/wa2p-c522.

Table 3
Priors for and Results from our MCMC Modeling of the RV and the Photometric TESS Data

Parameter (Unit)	Prior	RV Result	TESS Phot. Result
K (m s^{-1})	$\mathcal{N}(165.3, 4.3)$	162.5 ± 1.5	⋯
$\sqrt{e} \cos \omega$	$\mathcal{N}(0.0, 0.3)$	-0.171 ± 0.015	⋯
$\sqrt{e} \sin \omega$	$\mathcal{N}(0.0, 0.3)$	0.152 ± 0.029	⋯
$v \sin i$ (m s^{-1})	$\mathcal{N}(6300, 700)$	6714.1 ± 251.8	⋯
λ (°)	$\mathcal{U}(-180, 180)$	-1.05 ± 11.31	⋯
u_1	$\mathcal{N}(0.43, 0.15)$	0.787 ± 0.109	0.214 ± 0.186
u_2	$\mathcal{N}(0.24, 0.15)$	0.400 ± 0.138	0.070 ± 0.215
$a\,R_\star^{-1}$	$\mathcal{N}(14.2, 0.4)$	14.04 ± 0.28	13.9 ± 0.07
b	$\mathcal{N}(0.13, 0.17)$	0.036 ± 0.092	0.274 ± 0.047
$R_p\,R_\star^{-1}$	$\mathcal{N}(0.078, 0.001)$	0.0780 ± 0.0010	0.0760 ± 0.0017
T_c (days)	$\mathcal{N}(9297.11711, 0.00077)$	9297.11710 ± 0.00076	9297.11711 ± 0.00077
P (days)	$\mathcal{N}(9.289711, 0.000019)$	9.289718 ± 0.000005	9.289711 ± 0.000019
γ_{H1} (km s^{-1})	$\mathcal{U}(17.0, 17.5)$	17260.1 ± 1.2	⋯
γ_{H2} (km s^{-1})	$\mathcal{U}(17.0, 17.5)$	17237.5 ± 0.9	⋯
γ_{HN} (km s^{-1})	$\mathcal{U}(17.0, 17.5)$	17259.9 ± 1.2	⋯
γ_{CO} (km s^{-1})	$\mathcal{U}(17.0, 17.5)$	17248.1 ± 4.3	⋯
γ_{SO} (km s^{-1})	$\mathcal{U}(17.0, 17.5)$	17190.7 ± 5.7	⋯

Note. In the case of a normal (Gaussian) distribution ($\mathcal{N}$), the values within the brackets refer to the mean and standard deviation, respectively. For the uniform distribution ($\mathcal{U}$), the values refer to the lower and upper boundaries. The prior values are derived from those stated in Smith et al. (2014) and Borsato et al. (2021) for WASP-106 b, except for T_c and P, which were determined in this paper using the TESS photometry. The quadratic limb-darkening parameters were derived from the V- and y-band theoretical values from Claret et al. (2013), which are a close match to the HARPS/HARPS-N wavelength range. T_c is given in BJD$_{TDB}$−2450000. The subscripts "H1," "H2," "HN," "CO," and "SO" stand for HARPS first observation, HARPS second observation, HARPS-N, CORALIE, and SOPHIE, respectively.

allowing all possible values (see Table 3). The limb-darkening parameters were taken from Claret et al. (2013) with the closest passband in the case of the HARPS and HARPS-North spectrographs being the V and y bands; both of which are almost identical to each other for our stellar parameters.

3.2. TESS Photometry

We model the TESS photometry using the Transit and Light Curve Modeller, version 12 (TLCM; Csizmadia 2020). TLCM is a modeling code that allows analysis, fitting, and simulation of light curves of transiting exoplanets, as well as radial velocities. The code employs the Mandel & Agol (2002) descriptions of transits and occultations, with numerous other effects also being taken into account. Additionally, it has a wavelet implementation to deal with the red noise component in light curves, using the Carter & Winn (2009) model. The global minimum of the χ^2 or $\log L$ values are searched for by a genetic algorithm, with a subsequent refinement of the fit by an annealing algorithm. Error estimation is handled by a (differential evolution) Markov chain Monte Carlo algorithm.

TLCM takes the light curves as an input and fits for the epoch of the transit, orbital period (if multiple transits are available), semimajor axis, planet-to-star radius ratio, impact parameter, and the limb-darkening parameters. In this regard, we mainly fit for the orbital period and midtransit time to use them as priors for our RV modeling. Input parameters for our system were taken from TEPCat (Southworth 2011).

We also tried searching the TESS photometry for evidence of rotational variability. Using Lomb–Scargle periodograms, we searched the whole TESS light curve, as well as each sector separately (after removing the transits) for periodic modulations. This search yielded no conclusive rotation period for WASP-106 (Smith et al. 2014 also found no rotational variability), and so we are unable to convert our sky-projected obliquity to a true obliquity measurement.

4. Results

Using TLCM to fit the TESS data, we obtain the midtransit time and orbital period reported in Table 3 to use them as priors for the fit to the RV data. A plot of the phase-folded data and model are shown in Figure 1.

The results from the MCMC optimization for the RV data are given in Table 3. From our RV fit, we find a small eccentricity with:

$$\sqrt{e} \cos \omega = -0.171 \pm 0.015$$
$$\sqrt{e} \sin \omega = 0.152 \pm 0.028.$$

Solving this system of equations leads to $e = 0.05 \pm 0.01$. To test whether the elliptical or circular orbit is the preferred solution, we repeat the fit to the radial velocity data with the eccentricity fixed at zero. Comparing the Bayesian information criterion (BIC) values for the respective fits, we obtain $\mathrm{BIC}_c = 8632$ for the circular orbit and $\mathrm{BIC}_e = 8100$, indicating that the eccentric orbit is preferred. To further validate this result, we employ the F-test of Lucy & Sweeney (1971), and find a probability of just 1.7% for the apparent eccentricity to be spurious. According to their limit of 5% and in combination with the other evidence, we conclude that there is only a very small chance that the measured eccentricity could arise from a truly circular orbit, and hence we adopt the eccentric solution.

Aside from this, and as our main result, we find the projected stellar obliquity to be $\lambda = (-1 \pm 11)°$. This means that the stellar spin axis is aligned with the planetary orbital axis. Furthermore, we improve the uncertainties on some of the previously measured parameters from the aforementioned studies of this system, including a more precise measurement of the RV semiamplitude as well as an updated orbital period.

The full Keplerian orbit in the RVs is shown in Figure 2 together with the residuals from the fit. A zoom in of the RM anomaly is shown in Figure 3. The effect is clearly visible.

3
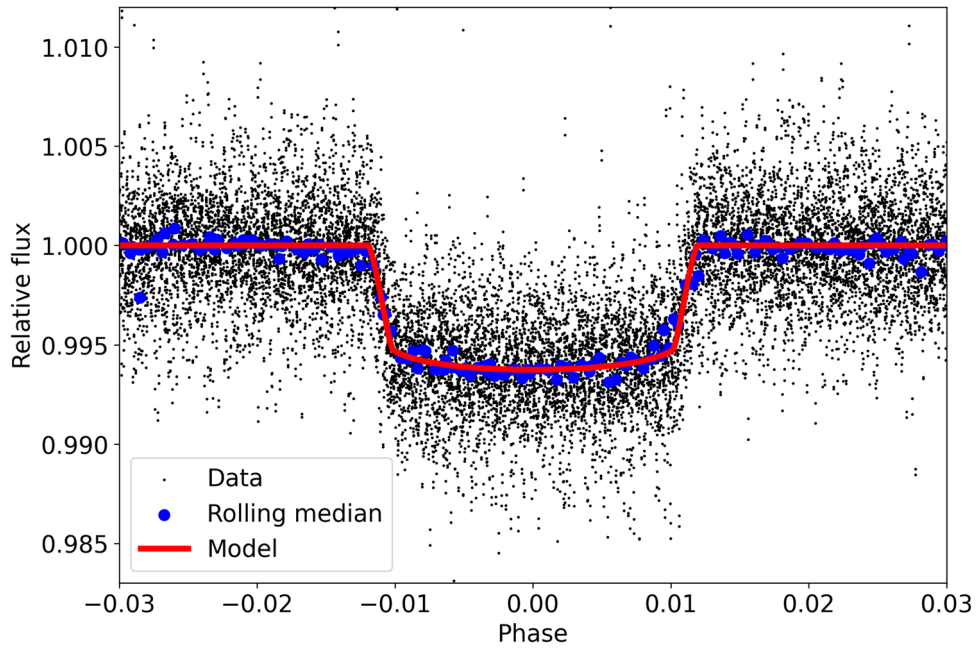
Figure 1. Phase-folded transit for all available TESS sectors. The TESS data is shown as black dots, the rolling median is shown as blue dots, and the final TLCM model is shown in red.
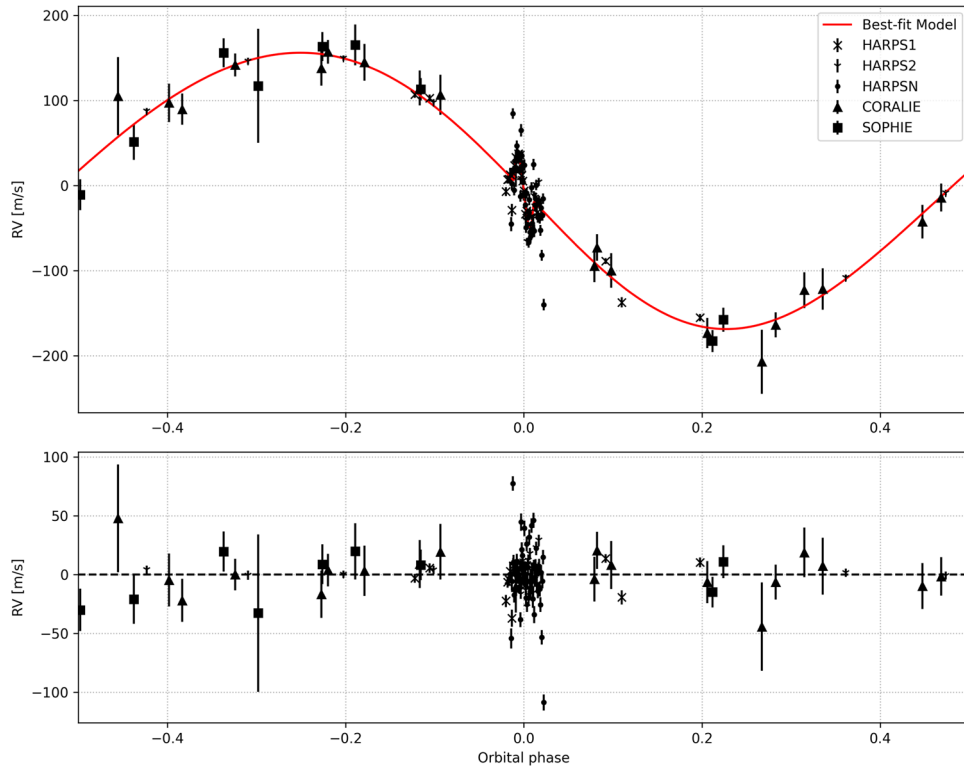
Figure 2. Top: RVs and the best-fit model for all of our data sets of WASP-106, showing the Keplerian orbit. The orbital phase is shown on the *x*-axis, with the radial velocity being shown on the *y*-axis. The different instruments are marked according to the legend, with "HARPS1" and "HARPS2" describing the first and second observation made with the HARPS spectrograph. The best-fit model is shown as the red curve. Bottom: residuals of our best-fitting model.

5. Discussion

From our measurement of the stellar obliquity angle λ, we find the system to be aligned. This is in accordance with the trend that was observed in single star systems by Rice et al. (2022b). The true 3D obliquity ψ of the system could be different however, since we can only measure the sky projection of this angle using the technique in this paper. The relatively large error bar that we obtain from our measurement is mainly caused by the scatter in the RVs during transit. A possible cause of this could be clouds during the observations.
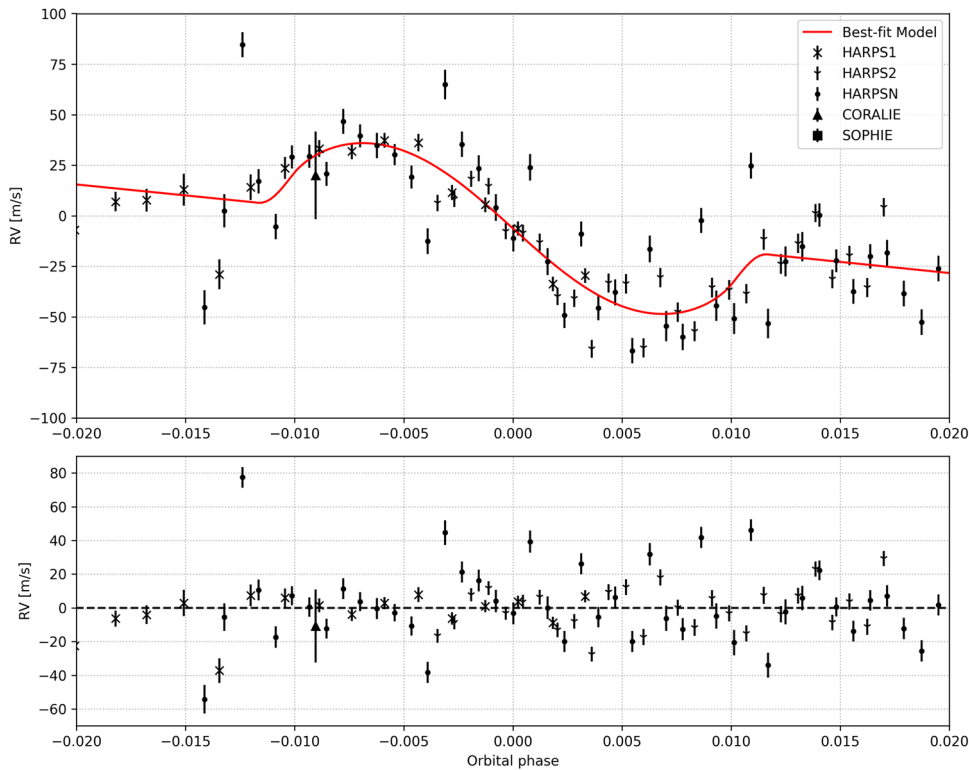
Figure 3. Same as Figure 2, but zoomed in on the Rossiter–McLaughlin anomaly.

It seems like that for both of the nights in early 2015, there were passing clouds in the sky,[11] which could have impaired the observations and led to the greater scatter for the data sets labeled as "HARPS2" and "HARPSN" in Figure 3. This scatter hinders a more precise retrieval of the obliquity angle λ. Removing both affected data sets, leaving only the first night of the HARPS RM observations (and a single CORALIE measurement), which covers approximately three quarters of the full transit, results in $\lambda = (-6.73 \pm 16.97)^{\circ}$. This result is consistent with the result from the fit to the full data set, and so is also consistent with alignment. Upon searching the residual RVs for additional periodic trends after subtracting our best-fit model, we find no additional signals that could correspond to further planets in the system.

The relatively small measured eccentricity, which we validated by comparing BIC values of two fits with free and fixed eccentricities and also the F-test of Lucy & Sweeney (1971), is an indication for the planetary orbit to be largely unaffected by tidal interactions between the planet and its host star, which could be an indication for our measured projected obliquity to be primordial. This supports the hypothesis of quiescent migration through the disk for warm Jupiters, in contrast to hot Jupiters, which are believed to get into their tight orbits via high-eccentricity migration due to interactions with other bodies in the early system (see e.g., Albrecht et al. 2022; Rice et al. 2022a, 2022b). Even though we delivered the first measurement of the spin–orbit alignment in this system, it will likely not be the last, since new observations were recently

taken using ESPRESSO. These measurements should be able to constrain λ even more. Aside from using the HARPS DRS RV data, we also extracted the RVs using SERVAL, which leads to a similar value of λ with an equally sized error bar.

We provide updated radial velocity and transit parameters, which are mostly consistent with those from the literature within 1σ. In more detail, for our determined RV semiamplitude (K), we find an uncertainty that is about a third compared to the value found in Smith et al. (2014). This improvement on the uncertainty is mainly driven by the few HARPS data points that extend beyond the transit phase of the planet. The same is the case for our measurement of the stellar rotational velocity ($v \sin i$). Since we do not fix the eccentricity in the RV fit, due to the availability of more measurements that have been taken in the meanwhile, we find a nonzero eccentricity at $e = 0.05$, in comparison to previous studies of this system. Moreover, our retrieved values for the scaled semimajor axis ($a\,R_\star^{-1}$) and impact parameter (b) from the RV data and the photometric data from TESS are in good agreement with each other and with those from Smith et al. (2014), but they only agree with the values of Borsato et al. (2021) within 4σ and 6σ, respectively. However, the high impact parameter from the latter study compensates for the lower semimajor axis value, caused by the well known degeneracy between the two parameters (see e.g., Alexoudi et al. 2020). Apart from the good agreement of the planet-to-star radius ratio ($R_P R_\star^{-1}$), the transit center time (T_c), and the orbital period (P)—for the latter of which we now find a smaller uncertainty—there is a small difference between the systemic velocities measured here and in Smith et al. (2014). Mainly, we find greater error bars for the offsets of CORALIE and SOPHIE. Nevertheless, their RV offsets lie within 1σ of our determined offsets. The values we find from our analysis of the TESS data with TLCM are in

---

[11] Based on the seeing (2015 January; https://www.not.iac.es/weather/dimm_index.php?day=16&month=01&year=2015&submit=Raw+Data; 2015 February; https://www.not.iac.es/weather/dimm_index.php?day=13&month=02&year=2015&submit=Raw+Data) and according to the historical weather data website timeanddate.com.

good agreement with those of Borsato et al. (2021). Our derived midtransit time is within 2σ of their value, although they have a slightly smaller uncertainty because of the more precise CHEOPS data that they used in their analysis. The orbital periods agree well within 1σ. However, we are able to further improve the uncertainty of the latter due to the many transits that are available in the TESS data.

6. Conclusions

From our analysis of three separate radial velocity data sets during transit of WASP-106 b in front of its host star—two of which were taken with HARPS, and one of which was taken with HARPS-N—we provide the first measurement of the stellar obliquity in this system, with $\lambda = (-1 \pm 11)°$, indicating good alignment between the stellar spin axis and the planetary orbital axis. This is in good agreement with the findings of Wright et al. (2023), who made use of newly acquired NEID spectra for their measurement and submitted their article nearly at the same time as us. More precise radial velocity measurements during transit of the planet might be able to put even tighter constraints on the orbital obliquity in this system, since the two HARPS RM observations only cover the first and the second half of the observed transit, respectively. The measurements from the second observation taken with HARPS, and those from HARPS-N show in addition to this scatter in the second half of the transit, which limits the precision with which the orbital obliquity can be inferred. This scatter could be caused by the presence of clouds, as the weather data suggest.

Our work adds another aligned system to the sample of 16 warm Jupiter systems with measured spin–orbit angles. Of these, 14 are aligned and two are misaligned at about $-30°$ (HAT-P-17, Mancini et al. 2022) and $40°$ (TOI-1859, Dong et al. 2023). Some of these planets, even though they show alignment, have nonzero eccentricities. These can usually be attributed to undetected companion bodies in the system. The same could be the case for our system with the small, but nonzero eccentricity for the planet's orbit that we find at high confidence, which is validated by the BIC values of respective fits, and also the Lucy & Sweeney (1971) F-test for small eccentricities. However, by examining the Lomb–Scargle periodogram (Lomb 1976; Scargle 1982), we do not find signs of other bodies. Given the moderate orbital period of about 9.3 days, the eccentricity damping timescale may be relatively long for WASP-106 b, making it possible for the eccentricity to be of primordial origin. This supports the theory that warm Jupiters migrate quiescently through the disk, in contrast to hot Jupiters that are thought to get into their tight orbits via high-eccentricity migration.

Acknowledgments

Appendix
Radial Velocity Data

The radial velocity data underlying this article can be found in Table 4.

Table 4
Radial Velocity Data of WASP-106 b

Time (days)	RV (km s^{-1})	Error (km s^{-1})	Observation
6298.61990	17.033000	0.014000	1
6329.63330	17.242000	0.021000	1
6330.56960	17.347000	0.017000	1
6331.59700	17.354000	0.017000	1
6360.49150	17.304000	0.013000	1
6363.53450	17.008000	0.013000	1
6364.68432	17.126600	0.024250	2
6365.72574	17.205720	0.019670	2
6366.62637	17.353310	0.045860	2
6368.74628	17.385940	0.020170	2
6369.77261	17.362930	0.020360	2
6370.77349	17.268240	0.021700	2
6371.59523	17.153570	0.018930	2
6371.76896	17.148240	0.020370	2
6372.76894	17.074720	0.017800	2
6373.78397	17.125310	0.021030	2
6377.37630	17.308000	0.067000	1
6378.38890	17.356000	0.024000	1
6403.39260	17.180000	0.018000	1
6410.50052	17.041100	0.037690	2
6423.58725	17.390130	0.013520	2
6424.55331	17.405420	0.013750	2
6438.51331	17.084330	0.014740	2
6441.47794	17.345440	0.022550	2
6443.51263	17.392980	0.021490	2
6449.52837	17.234020	0.016300	2
6469.48415	17.337830	0.018350	2
6481.46628	17.354740	0.023680	2
6696.76093	17.175350	0.015760	2
6750.59786	17.366900	0.003779	3
6750.75405	17.362900	0.004046	3
6751.54932	17.253000	0.005156	3
6751.56677	17.267100	0.004778	3
6751.57991	17.267800	0.005576	3
6751.59571	17.273000	0.007835	3
6751.61093	17.231100	0.007376	3
6751.62421	17.274200	0.006412	3
6751.63890	17.283700	0.005411	3
6751.65343	17.293300	0.004182	3
6751.66727	17.291900	0.003870	3

---

[12] http://www.astropy.org

Table 4
(Continued)

Time (days)	RV (km s^{-1})	Error (km s^{-1})	Observation
6751.68125	17.297400	0.003607	3
6751.69565	17.296200	0.004319	3
6751.70992	17.271600	0.003740	3
6751.72418	17.265500	0.003590	3
6751.73801	17.253800	0.003509	3
6751.75282	17.226300	0.003559	3
6751.76665	17.230500	0.003609	3
6752.59058	17.171300	0.003583	3
6752.75786	17.122600	0.006005	3
6753.57398	17.104900	0.004204	3
7033.78505	17.129400	0.003421	4
7034.82784	17.229000	0.003252	4
7035.78606	17.325100	0.003365	4
7036.84025	17.383800	0.003938	4
7037.83560	17.387300	0.003011	4
7038.77477	17.335300	0.003641	4
7039.68490	17.243700	0.004058	4
7039.69209	17.245800	0.004005	4
7039.69934	17.255700	0.003966	4
7039.70678	17.252100	0.004099	4
7039.71402	17.229800	0.003994	4
7039.72127	17.228900	0.004167	4
7039.72852	17.224300	0.004361	4
7039.73604	17.197600	0.004329	4
7039.74316	17.196600	0.004313	4
7039.75061	17.171600	0.004430	4
7039.75779	17.204200	0.004678	4
7039.76526	17.203800	0.004747	4
7039.77263	17.172200	0.004725	4
7039.77982	17.206900	0.004758	4
7039.78726	17.189800	0.004773	4
7039.79444	17.180300	0.004962	4
7039.80183	17.202000	0.004882	4
7039.80914	17.200800	0.004851	4
7039.81638	17.198900	0.004816	4
7039.82385	17.225800	0.005114	4
7039.83109	17.213700	0.004898	4
7039.83848	17.223800	0.004747	4
7039.84581	17.238800	0.004507	4
7039.85297	17.206200	0.004647	4
7039.86030	17.217800	0.004858	4
7039.86782	17.201900	0.004709	4
7039.87485	17.241600	0.004556	4
7067.45494	17.214500	0.008478	5
7067.46341	17.262300	0.008211	5
7067.47106	17.344400	0.006175	5
7067.47799	17.276900	0.006085	5
7067.48528	17.254500	0.006337	5
7067.49218	17.288900	0.005686	5
7067.49953	17.289300	0.005745	5
7067.50681	17.280600	0.005943	5
7067.51400	17.306500	0.006212	5
7067.52121	17.299400	0.005694	5
7067.52830	17.294600	0.006239	5
7067.53587	17.290100	0.005165	5
7067.54307	17.279000	0.005667	5
7067.54993	17.247300	0.006303	5
7067.55735	17.324800	0.007338	5
7067.56451	17.295200	0.006260	5
7067.57171	17.283300	0.006428	5
7067.57894	17.263900	0.006614	5
7067.58634	17.248800	0.006575	5
7067.59357	17.283800	0.006579	5
7067.60091	17.237200	0.006699	5
7067.60812	17.210600	0.006265	5
7067.61531	17.250800	0.006215	5
7067.62263	17.214200	0.006029	5
7067.62974	17.222000	0.006404	5
7067.63704	17.193100	0.006250	5
7067.64444	17.243400	0.006597	5
7067.65143	17.205200	0.007483	5
7067.65846	17.199900	0.006507	5

Table 4
(Continued)

Time (days)	RV (km s^{-1})	Error (km s^{-1})	Observation
7067.66630	17.257500	0.006203	5
7067.67276	17.215400	0.007515	5
7067.68041	17.209000	0.007598	5
7067.68754	17.284600	0.006480	5
7067.69477	17.206500	0.007343	5
7067.70217	17.237200	0.007430	5
7067.70942	17.244600	0.007264	5
7067.71668	17.260200	0.005846	5
7067.72383	17.237600	0.005626	5
7067.73110	17.222400	0.006139	5
7067.73823	17.239800	0.006056	5
7067.74544	17.241600	0.006365	5
7067.75258	17.221400	0.006386	5
7067.76016	17.207200	0.006372	5
7067.76760	17.233700	0.006322	5
7067.77435	17.177800	0.006230	5
7067.78161	17.224800	0.006180	5
7067.78878	17.244300	0.006133	5
7067.79602	17.119800	0.006872	5

Note. The "Observation" column refers to 1 to 5 of the data sets from SOPHIE, CORALIE, HARPS (First Night), HARPS (Second Night), and HARPS-N, respectively. Time is given in BJD$_{TDB}$−2450000.

ORCID iDs

Jan-Vincent Harre ⓘ https://orcid.org/0000-0001-8935-2472
Alexis M. S. Smith ⓘ https://orcid.org/0000-0002-2386-4341
Teruyuki Hirano ⓘ https://orcid.org/0000-0003-3618-7535
Szilárd Csizmadia ⓘ https://orcid.org/0000-0001-6803-9698
Amaury H. M. J. Triaud ⓘ https://orcid.org/0000-0002-5510-8751
David R. Anderson ⓘ https://orcid.org/0000-0001-7416-7522

References

Ahlers, J. P., Johnson, M. C., Stassun, K. G., et al. 2020, AJ, 160, 4
Albrecht, S., Winn, J. N., Butler, R. P., et al. 2012, ApJ, 744, 189
Albrecht, S. H., Dawson, R. I., & Winn, J. N. 2022, PASP, 134, 082001
Alexoudi, X., Mallonn, M., Keles, E., et al. 2020, A&A, 640, A134
Anderson, D. R., Triaud, A. H. M. J., Turner, O. D., et al. 2015, ApJL, 800, L9
Astropy Collaboration, Price-Whelan, A. M., Lim, P. L., et al. 2022, ApJ, 935, 167
Astropy Collaboration, Price-Whelan, A. M., Sipőcz, B. M., et al. 2018, AJ, 156, 123
Astropy Collaboration, Robitaille, T. P., Tollerud, E. J., et al. 2013, A&A, 558, A33
Bayliss, D. D. R., Winn, J. N., Mardling, R. A., & Sackett, P. D. 2010, ApJL, 722, L224
Borsato, L., Piotto, G., Gandolfi, D., et al. 2021, MNRAS, 506, 3810
Bourrier, V., Attia, O., Mallonn, M., et al. 2023, A&A, 669, A63
Carter, J. A., & Winn, J. N. 2009, ApJ, 704, 51
Cegla, H. M., Lovis, C., Bourrier, V., et al. 2016, A&A, 588, A127
Claret, A., Hauschildt, P. H., & Witte, S. 2013, A&A, 552, A16
Cosentino, R., Lovis, C., Pepe, F., et al. 2012, Proc. SPIE, 8446, 84461V
Crouzet, N., McCullough, P. R., Long, D., et al. 2017, AJ, 153, 94
Csizmadia, S. 2020, MNRAS, 496, 4442
Dong, J., Wang, S., Rice, M., et al. 2023, ApJL, 951, 29
Doyle, L., Cegla, H. M., Anderson, D. R., et al. 2023, MNRAS, 522, 4499
Esposito, M., Covino, E., Desidera, S., et al. 2017, A&A, 601, A53
Esposito, M., Covino, E., Mancini, L., et al. 2014, A&A, 564, L13
Foreman-Mackey, D., Hogg, D. W., Lang, D., & Goodman, J. 2013, PASP, 125, 306
Fulton, B. J., Howard, A. W., Winn, J. N., et al. 2013, ApJ, 772, 80
Gray, D. F. 1977, ApJ, 218, 530
Gray, D. F. 2018, ApJ, 857, 139
Hébrard, G., Ehrenreich, D., Bouchy, F., et al. 2011, A&A, 527, L11
Hirano, T., Suto, Y., Winn, J. N., et al. 2011, ApJ, 742, 69

Harre et al.

Hixenbaugh, K., Wang, X.-Y., Rice, M., & Wang, S. 2023, ApJL, 949, L35
Kraft, R. P. 1967, ApJ, 150, 551
Lomb, N. R. 1976, Ap&SS, 39, 447
Lucy, L. B., & Sweeney, M. A. 1971, AJ, 76, 544
Lund, M. B., Rodriguez, J. E., Zhou, G., et al. 2017, AJ, 154, 194
Mancini, L., Esposito, M., Covino, E., et al. 2022, A&A, 664, A162
Mandel, K., & Agol, E. 2002, ApJL, 580, L171
Mayor, M., Pepe, F., Queloz, D., et al. 2003, Msngr, 114, 20
McLaughlin, D. B. 1924, ApJ, 60, 22
Perruchot, S., Kohler, D., Bouchy, F., et al. 2008, Proc. SPIE, 7014, 70140J
Queloz, D., Mayor, M., Weber, L., et al. 2000, A&A, 354, 99
Rice, M., Wang, S., & Laughlin, G. 2022a, ApJL, 926, L17

Rice, M., Wang, S., Wang, X.-Y., et al. 2022b, AJ, 164, 104
Rossiter, R. A. 1924, ApJ, 60, 15
Scargle, J. D. 1982, ApJ, 263, 835
Sedaghati, E., Jordán, A., Brahm, R., et al. 2023, AJ, 166, 130
Smith, A. M. S., Anderson, D. R., Armstrong, D. J., et al. 2014, A&A, 570, A64
Southworth, J. 2011, MNRAS, 417, 2166
Winn, J. N., Fabrycky, D., Albrecht, S., & Johnson, J. A. 2010, ApJL, 718, L145
Wong, I., Shporer, A., Zhou, G., et al. 2021, AJ, 162, 256
Wright, J., Rice, M., Wang, X.-Y., et al. 2023, arXiv:2308.07532
Zechmeister, M., Reiners, A., Amado, P. J., et al. 2018, A&A, 609, A12